Expression and Characterization of the Catalytic Domains of Soluble Guanylate Cyclase: Interaction with the Heme Domain†

Jonathan A. Winger‡ and Michael A. Marletta*,‡,§

Department of Medicinal Chemistry, The University of Michigan, Ann Arbor, Michigan 48109-0606, and Department of Chemistry, Department of Molecular and Cell Biology, Division of Physical Biosciences, Lawrence Berkeley National Laboratory, University of California, Berkeley 94720-1460

Received November 12, 2004; Revised Manuscript Received December 16, 2004

ABSTRACT: The catalytic domains (α_{cat} and β_{cat}) of $\alpha1\beta1$ soluble guanylate cyclase (sGC) were expressed in *Escherichia coli* and purified to homogeneity. α_{cat}, β_{cat}, and the $\alpha_{cat}\beta_{cat}$ heterodimeric complex were characterized by analytical gel filtration and circular dichroism spectroscopy, and activity was assessed in the absence and presence of two different N-terminal regulatory heme-binding domain constructs. α_{cat} and β_{cat} were inactive separately, but together the domains exhibited guanylate cyclase activity. Analysis by gel filtration chromatography demonstrated that each of the approximately 25-kDa domains form homodimers. Heterodimers were formed when α_{cat} and β_{cat} were combined. Results from circular dichroism spectroscopy indicated that no major structural changes occur upon heterodimer formation. Like the full-length enzyme, the $\alpha_{cat}\beta_{cat}$ complex was more active in the presence of Mn^{2+} as compared to the physiological cofactor Mg^{2+}, although the magnitude of the difference was much larger for the catalytic domains than for the full-length enzyme. The K_M for Mn^{2+}-GTP was measured to be 85 ± 18 μM, and in the presence of Mn^{2+}-GTP, the K_D for the $\alpha_{cat}\beta_{cat}$ complex was 450 ± 70 nM. The N-terminal heme-bound regulatory domain of the $\beta1$ subunit of sGC inhibited the activity of the $\alpha_{cat}\beta_{cat}$ complex in trans, suggesting a domain-scale mechanism of regulation by NO. A model in which binding of NO to sGC causes relief of an autoinhibitory interaction between the regulatory heme-binding domain and the catalytic domains of sGC is proposed.

The principle physiological receptor for nitric oxide (NO) when functioning as a signaling agent is soluble guanylate cyclase (sGC,[1] EC 4.6.1.2) (*1*−*5*). sGC catalyzes a cyclization reaction in which guanosine 5′-triphosphate (GTP) is converted into the 3′,5′-cyclic monophosphate second messenger, cGMP. The product cGMP elicits downstream effects that ultimately result in phenomena such as smooth muscle relaxation and vasodilation (*6*). An understanding of the molecular details of mechanism and regulation of sGC is of interest in developing therapeutic strategies for the treatment of NO/cGMP signaling pathway-related disease.

sGC is a heterodimeric heme-containing protein consisting of α and β subunits. Each subunit contains a conserved N-terminal regulatory domain (*7*) predicted to exhibit a novel structure (*8*), the H−NOX (heme−nitric oxide/oxygen binding) fold. It is this domain to which the heme is bound in the β subunit of the sGC $\alpha1\beta1$ heterodimer. Upon binding of NO to the heme, the enzyme is activated several hundred fold above the basal level (*9*, *10*). The changes induced in the sGC heme environment by the binding of NO are thought to be responsible for initiating the events that result in enzyme activation; however, the exact mechanism of activation remains unclear. The corresponding N-terminal region of the $\alpha1$ subunit is homologous to the N-terminus of the $\beta1$ subunit and likely represents a similar fold despite the inability to bind heme. sGC truncations consisting solely of the $\beta1$ H−NOX domain appear monomeric (D. S. Karow, J. H. Davis, and M. A. Marletta, manuscript in preparation), and the corresponding domain of the $\alpha1$ subunit can be deleted from the full-length enzyme with little effect on enzyme activity (*11*), indicating that the H−NOX domains are not likely to be involved in dimerization. Each subunit also contains a central region of unknown function consisting of a domain predicted to adopt a PAS fold and an amphipathic helical domain (*7*). Recent evidence suggests that these central domains are involved in sensitivity to NO and the exogenous activator, YC-1 (*11*), and in hetero- and homo-

† Funding was provided by the LDRD Fund from LBNL to M.A.M. and by an Eli Lilly Fellowship, a Pharmaceutical Sciences Training Program Fellowship (grant number GM07767 NIGMS), and an American Foundation for Pharmaceutical Education Fellowship to J.A.W.

* To whom correspondence should be addressed at University of California, Berkeley, Department of Chemistry, 211 Lewis Hall, Berkeley, CA 94720-1460. Phone: (510) 643−9325; fax: (510) 643-9388; e-mail: marletta@berkeley.edu.

‡ University of Michigan.

§ University of California.

[1] Abbreviations: sGC, soluble guanylate cyclase; NO, nitric oxide; GTP, guanosine 5′-triphosphate; cGMP, guanosine 3′,5′-cyclic monophosphate; PAS, protein fold first identified in the *P*er, *A*rnt, and *S*im proteins; AC, adenylate cyclase; α_{cat}, the catalytic domain of the sGC $\alpha1$ subunit; β_{cat}, the catalytic domain of the sGC $\beta1$ subunit; *E. coli*, *Escherichia coli*; IPTG, isopropyl-β-D-thiogalactopyranoside; DEA/NO, diethylammonium (*Z*)-1-(*N*,*N*-diethylamino)diazen-1-ium-1,2-diolate; SDS−PAGE, sodium dodecyl sulfate-polyacrylamide gel electrophoresis; DEA, diethanolamine; DTT, dithiothreitol; HEPES, 4-(2-hydroxyethyl)-1-piperazineethane sulfonic acid; PVDF, polyvinylidene fluoride; Tris, 2-amino-2-(hydroxymethyl)-1,3-propanediol; PCR, polymerase chain reaction; EIA, enzyme immunoassay.

10.1021/bi047601d CCC: $30.25
Published on Web 02/17/2005

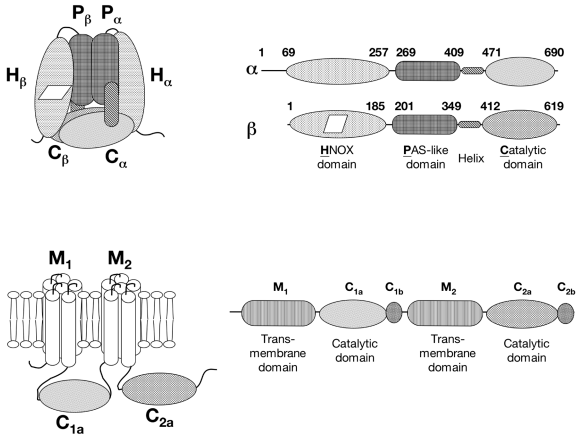

FIGURE 1: Comparison between soluble guanylate cyclase and mammalian adenylate cyclase. Depicted on the left are models of the two proteins, and shown on the right are schematics of the proposed domain organizations for each enzyme. (A) Model and schematic for sGC. The domains of sGC are labeled by the first letters of their domain names (underlined). The sGC heme is represented by the white parallelogram on the β1 subunit. (B) Model and schematic for mammalian AC. The regions of mammalian AC are labeled according to convention (*40*).

dimerization (*12*). At the C-terminus of each subunit is found a consensus nucleotide cyclase catalytic domain (*13*). The sequences of the two ~25 kDa catalytic domains of sGC (α_{cat} and β_{cat}) share ~60% homology and are also homologous to the C_1 and C_2 catalytic domains of the mammalian adenylate cyclases (AC) (*14*, *15*). Taken together, these observations can be used to construct an updated model of the domain organization of sGC (Figure 1A).

Full-length sGC is generally obtained from tissue or from baculovirus/insect cell expression systems (*16*−*21*). However, these methods result in the isolation of small amounts of labile protein. Expression in *E. coli*, a preferred method for obtaining large amounts of protein for study, has been unsuccessful to date. Expression of the domains of a protein is a common way to facilitate biochemical and structural analysis of proteins that are difficult to obtain in adequate amounts. Several constructs containing the N-terminal heme-binding domain of the β1 subunit of sGC, which contain a heme with ligand-binding properties identical to those of the full-length enzyme, have been expressed, purified, and characterized in this manner (*22*) (D. S. Karow, J. H. Davis, and M. A. Marletta, manuscript in preparation). This method has also been used in the study of the catalytic domains of mammalian AC (*23*−*25*). In this work, we describe the separate expression and purification of the α_{cat} and β_{cat} domains of rat $\alpha1\beta1$ sGC from *E. coli*, the characterization of the oligomerization and activity of each domain separately and together, and the inhibition of the activity of the $\alpha_{cat}\beta_{cat}$ complex by two different sGC heme-binding domain constructs.

EXPERIMENTAL PROCEDURES

Materials. Plasmids carrying the rat lung sGC α1 and β1 cDNAs were a gift from Dr. Masaki Nakane, Abbott Laboratories. The plasmid pGroE was a gift from Dr. Arthur Horwich, Yale University. Primers, 2xYT, Luria Broth (LB), and precast 10−20% Tris-glycine gels were obtained from Invitrogen Corp. NiNTA-agarose Superflow resin was purchased from Qiagen. The plasmid pET-24a and *E. coli* Tuner(DE3) competent cells were obtained from Novagen. IPTG was purchased from Promega. All restriction enzymes were from New England Biolabs. DEA/NO was purchased from Cayman Chemical Co. All other chemicals were from Sigma unless otherwise indicated.

Construction of sGC α1 and β1 Catalytic Domain Constructs. The sequences of the catalytic domains from several adenylate and guanylate cyclases were aligned using MegAlign (DNASTAR, Inc.). The alignment was used to select start and end points for sGC α_{cat} and β_{cat} catalytic domain constructs, which consisted of residues 467−690[2] from the α1 subunit and residues 414−619 from the β1 subunit. For both α_{cat} and β_{cat}, PCR was used to introduce a *HindIII* site, a ribosome-binding site, and an in-frame ATG start codon upstream from the desired cDNA sequences for each construct. An *XhoI* site was introduced at the C-terminus of each construct to facilitate the incorporation of a vector-derived hexa-His tag. The α_{cat} forward primer was 5′-GAAAGCTTAAGAAGGAGATATACATGCAAGGACAA-ATTGTGCAAGCCAAG-3′, and the reverse primer was 5′-AACTCGAGATCTACCCCTGATGC-3′. The β_{cat} forward primer was 5′-GAAAGCTTAAGAAGGAGATATACATG-GCCAAAAGATACGACAATGTGACC-3′, and the reverse primer was 5′-TTCTCGAGGTTTTCATCCTGGTTT-3′. The PCR products were cloned into pET-24a and sequenced to verify the presence of the desired changes (University of California, Berkeley DNA Sequencing Facility).

Expression of Catalytic Domains in E. coli. Plasmids pET24a/α_{cat} or pET24a/β_{cat} were transformed into *E. coli* Tuner(DE3) competent cells, along with the auxiliary plasmid pGroE. Starter cultures (150 mL of LB containing 34 μg/mL of kanamycin and 10 μg/mL of tetracycline) were inoculated from single colonies and were grown overnight at 37 °C. Expression cultures (12 × 1 L of 2xYT containing 34 μg/mL of kanamycin and 10 μg/mL of tetracycline) were each inoculated with 12 mL from the overnight cultures and were grown at 37 °C to an A_{600} of 0.5−0.6. The cultures were then cooled to 23 °C, and protein expression was induced by the addition of IPTG to a final concentration of 1 mM. Cells were harvested by centrifugation 15 h postinduction, and cell pellets were stored at −80 °C.

Purification of Individual sGC Catalytic Domains. All manipulations were carried out at 4 °C. Frozen cell pellets from 12-L expression cultures of either α_{cat} or β_{cat} were thawed and resuspended in buffer A [50 mM KH_2PO_4, pH 8.0, 300 mM NaCl, 25 mM imidazole, 5 mM β-mercaptoethanol, 1 mM Pefabloc (Pentapharm), 1 mM benzamidine, 10% glycerol] plus Complete EDTA-free protease inhibitor cocktail (Roche). Resuspended cells were brought to 10 mM $MgCl_2$, 0.1 mg/mL in DNase, and 0.5 mg/mL in lysozyme and placed on ice for 30 min. Cells were lysed by sonication for 30 s followed by disruption with an Emulsiflex-C5 high-pressure homogenizer (Avestin, Inc.). The lysate was centrifuged at 200 000*g* for 1.5 h, and the supernatant was applied to an 8-mL column of NiNTA-Agarose Superflow resin equilibrated with buffer A at a flow rate of 2 mL/min using a BioLogic LP (Bio-Rad Laboratories). The column

[2] sGC amino acid numbering is that of the rat enzyme unless otherwise noted.

was washed with buffer A until the A_{280} was stable, washed with 200 mL of 45 mM imidazole in buffer A, and eluted with 100 mL of 150 mM imidazole in buffer A, collecting 5-mL fractions during the elution. Fractions containing α_{cat} or β_{cat} were identified by A_{280}, pooled, concentrated to 0.5−1 mL in a Vivaspin-20 10K filter (Vivascience), and exchanged into buffer B (50 mM DEA, pH 8.5, 20 mM NaCl) by three consecutive 10-fold dilution/concentration cycles in a Vivaspin-20 10K filter. The sample was diluted to ~4 mL with buffer B and applied to a 2-mL prepacked POROS HQ2 anion-exchange column (Applied Biosystems) at 2 mL/min using a BioLogic Duo Flow (Bio-Rad Laboratories). The column was washed with 10 mL buffer B and developed with a 50 mL 20−400 mM gradient of NaCl in buffer B, collecting 1-mL fractions. Fractions containing purified α_{cat} or β_{cat} were identified by SDS−PAGE. Pooled fractions were concentrated in a Vivaspin-6 10K filter and stored at −80 °C. Protein purity was assessed by SDS−PAGE using precast 10−20% Tris-glycine gels and was routinely greater than 95%. Protein concentrations were determined using the Bradford Microassay (Bio-Rad Laboratories); bovine serum albumin was used as a standard.

Amino Acid Sequencing. N-Terminal amino acid sequences were determined by Edman degradation by the Protein Chemistry Laboratory at Texas A&M University, using a Hewlett-Packard G1000A Automated Protein Sequencer. SDS−PAGE was performed on purified α_{cat} or β_{cat} using a precast 10−20% Tris-glycine gel. Proteins were then transferred to a PVDF membrane (Bio-Rad Laboratories) by electroblot, and the membrane was stained with Coomassie Blue R-250 (Bio-Rad Laboratories) to visualize the protein bands. The bands were excised, dried, and submitted for analysis.

Activity of α_{cat} and β_{cat} Catalytic Domains. End-point assays at 37 °C were performed in triplicate as described previously (*26*). The assay mixtures contained 50 mM HEPES, pH 7.4, 6 mM $MgCl_2$ or $MnCl_2$, 3 mM GTP, and 2 mM DTT. Assay mixtures were equilibrated for 1 min at 37 °C, and reactions were initiated by addition of 5 μg of α_{cat}, 5 μg of β_{cat}, or 5 μg each of both catalytic domains. Reactions were quenched after 16−20 min by addition of 400 μL of 125 mM $Zn(CH_3CO_2)_2$ followed by 500 μL of 125 mM Na_2CO_3. cGMP formed was quantified with a cGMP EIA kit, Format B (Biomol), per the manufacturer's instructions. To determine the K_M for Mn^{2+}-GTP, activity in the presence of Mn^{2+} was measured as above, except the concentration of GTP was varied from 10 to 1000 μM. The resulting data were fit to the Michaelis−Menten equation to obtain the K_M.

Analytical Gel Filtration Studies on the α_{cat} and β_{cat} Catalytic Domains. Analytical gel filtration on α_{cat}, β_{cat}, and the $\alpha_{cat}\beta_{cat}$ complex was performed on a BioLogic Duo Flow (Bio-Rad Laboratories) equipped with a prepacked Superdex S200 HiLoad 16/60 gel filtration column (Pharmacia) at 4 °C. The buffer contained 50 mM HEPES, pH 7.4, 150 mM NaCl, and was run at a flow rate of 1 mL/min. The sample injection volume was 1 mL. The standards used were cytochrome *c* (12.4 kDa), carbonic anhydrase (29 kDa), ovalbumin (45 kDa), bovine serum albumin (66 kDa), yeast alcohol dehydrogenase (150 kDa), and thyroglobulin (669 kDa). All standards were 0.42 mg/mL upon loading. The sample concentrations upon loading were α_{cat}, 21 μM in monomer; β_{cat}, 56 μM in monomer; and $\alpha_{cat}\beta_{cat}$ complex, 8.9 μM. All proteins were detected by absorbance at 280 nm.

Circular Dichroism Spectroscopy Studies on the α_{cat} and β_{cat} Catalytic Domains. α_{cat} (8.1 μM in monomer), β_{cat} (8.3 μM in monomer), or $\alpha_{cat}\beta_{cat}$ complex (4 μM) were prepared in 20 mM Tris•HCl, pH 7.4, 100 mM NaCl. The circular dichroism spectrum of each sample was measured using a 1-mm path length cell at 37 °C on a Jasco J-810 CD spectrophotometer. Samples were equilibrated for 1 min before initiation of scans, and data were collected from 250 to 195 nm at 1 nm data intervals with 5 s averaging for each data point.

Determination of the K_D of the sGC $\alpha_{cat}\beta_{cat}$ Catalytic Domain Complex. End-point assays were performed at 37 °C in duplicate. The assay mixtures contained 50 mM HEPES, pH 7.4, 6 mM $MnCl_2$, 3 mM GTP, and 2 mM DTT. Assay mixtures were equilibrated for 1 min at 37 °C, and reactions were initiated by addition of varying amounts of $\alpha_{cat}\beta_{cat}$ complex. Reactions were quenched after 20 min, and cGMP formed was quantified by EIA. The activities at different $\alpha_{cat}\beta_{cat}$ concentrations were fit to a standard saturation equation, $v = V_{max}[\alpha_{cat}\beta_{cat}]/(K_D + [\alpha_{cat}\beta_{cat}])$ to obtain the K_D.

Purification of sGC Heme-Binding Domain Constructs. The rat sGC heme-binding domain constructs β1(1−194) and β1(1−385) were expressed and purified containing a stoichiometric amount of heme as described (Karow, D. S., Davis, J. H., and Marletta, M. A. manuscript in preparation) (*27*).

Inhibition of sGC $\alpha_{cat}\beta_{cat}$ Catalytic Domain Complex Activity by sGC Heme-Binding Domain Constructs. End-point assays were performed in duplicate with or without the addition of β1(1−194) or β1(1−385) heme-binding domain constructs. Assay mixtures contained 50 mM HEPES, pH 7.4, 6 mM $MgCl_2$, 3 mM GTP, 2 mM DTT, and β1(1−194) or β1(1−385) heme-binding domain constructs as indicated. Assay mixtures were equilibrated to 37 °C for 1 min, and reactions were initiated by addition of $\alpha_{cat}\beta_{cat}$ complex to 1.6 μM. Assays were quenched after 16 min and cGMP produced was quantified by EIA.

RESULTS AND DISCUSSION

Expression of α_{cat} and β_{cat}. The development of soluble catalytic domain constructs of mammalian AC has provided a useful system for the structural and biochemical study of a membrane-bound protein only available in small quantities (*23*, *28*). Such a system would also be useful for sGC, which contains a pair of catalytic domains homologous to those of AC (Figure 1B). sGC, typically expressed and purified using baculovirus/insect cell systems, is similarly difficult to express in large amounts. Additionally, efforts to express soluble, active full-length sGC in *E. coli* have been unsuccessful.[3] Using an alignment of the catalytic domains of AC with those of sGC, a hexa-histidine-tagged catalytic domain construct (designated α_{cat} or β_{cat}) was designed for each subunit of rat α1β1 sGC. α_{cat} and β_{cat} were each expressed in *E. coli* in the presence of the auxiliary plasmid pGroE, from which the chaperone proteins GroEL and GroES are

[3] Winger, J. A. and Marletta, M. A., unpublished results.

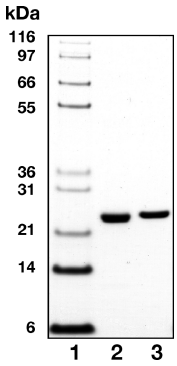

FIGURE 2: SDS−PAGE analysis of purified α_{cat} and β_{cat}. Protein samples were mixed with SDS loading buffer + reductant, boiled, and run on a 10−20% Tris-glycine gel. Lane 1, Mark 12 molecular weight markers; lane 2, α_{cat} (~1.5 μg); lane 3, β_{cat} (~1 μg).

expressed (*29*), in an effort to increase the amount of soluble protein produced. Most of the soluble α_{cat} and β_{cat} expressed was present as a complex with GroEL as determined by SDS−PAGE and gel filtration chromatography (data not shown). However, for both α_{cat} and β_{cat}, a small amount of soluble, uncomplexed protein was present and amenable to purification from the supernatant fraction of bacterial lysates. Expression of either catalytic domain in the absence of pGroE resulted in undetectable levels of soluble, uncomplexed α_{cat} or β_{cat}.

Purification of α_{cat} and β_{cat}. α_{cat} and β_{cat} were purified using nickel affinity chromatography and anion-exchange chromatography as described under Experimental Procedures. Both proteins were judged to be homogeneous by SDS−PAGE (Figure 2). Both α_{cat} and β_{cat} ran at ~25 kDa, close to the predicted molecular weights of 25.9 kDa (α_{cat}) and 24.1 kDa, (β_{cat}). Each protein was subjected to N-terminal amino acid sequencing by Edman degradation. The N-terminal amino acid sequence of each protein matched those predicted from the DNA sequences (α_{cat} retained the N-terminal methionine; β_{cat} did not), confirming the identity of the purified proteins. Yields from 12 L of *E. coli* were typically in the range of 0.4−1 mg for α_{cat} or 1−2 mg for β_{cat}.

Activity of Purified α_{cat}, β_{cat}, and $\alpha_{cat}\beta_{cat}$. In the presence of the physiological substrate Mg^{2+}-GTP, purified α_{cat} and β_{cat} displayed no activity by themselves, but exhibited enzymatic activity when combined (Figure 3A). A similar observation was reported for the AC catalytic domains (*24*, *25*). This result has an important implication for the functions of the various regions of sGC: it confirms that the catalytic regions of each subunit must heterodimerize to exhibit sGC activity. The results also clarify the accepted idea that the sGC subunits must be coexpressed to be active (*30*, *31*), indicating that, at least for the catalytic domains, each can fold to a stable conformation in the absence of its partner. The requirement for subunit coexpression for activity must therefore relate to folding in the regions N-terminal to the catalytic regions of the full-length enzyme.

In the presence of Mn^{2+}-GTP, purified α_{cat} and β_{cat} by themselves displayed a small amount of activity, but this activity was less than 1% of the activity exhibited by the $\alpha_{cat}\beta_{cat}$ complex (Figure 3B). The activity of $\alpha_{cat}\beta_{cat}$ was higher with Mn^{2+} than with Mg^{2+}. A similar phenomenon was observed with the full-length enzyme, which displayed

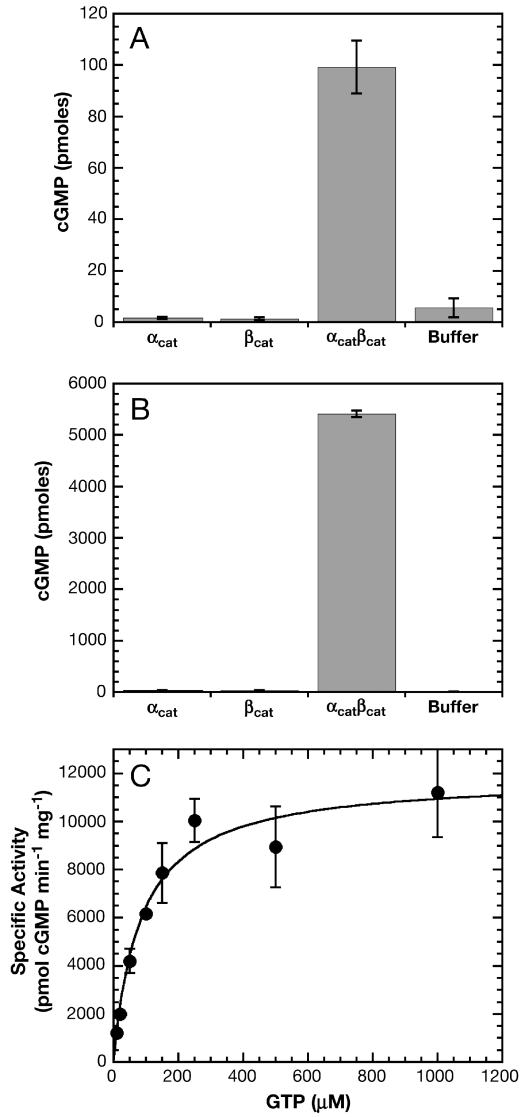

FIGURE 3: Activities of purified α_{cat}, β_{cat}, and the $\alpha_{cat}\beta_{cat}$ complex. Activity assays were carried out with α_{cat} alone (5μg), β_{cat} alone (5μg), or α_{cat} and β_{cat} together (5 μg of each). (A) Activity in the presence of Mg^{2+}. (B) Activity in the presence of Mn^{2+}. (C) Activity in the presence of increasing concentrations of GTP. The data were fit to the Michaelis−Menten equation to yield the K_M for Mn^{2+}-GTP.

a basal activity in the presence of Mn^{2+} roughly 8-fold higher than in the presence of Mg^{2+} (data not shown), consistent with reported values (*16*, *18*, *32*, *33*). However, the magnitude of the difference in specific activity because of the change in divalent cation was much larger for the isolated catalytic domains (~200-fold for $\alpha_{cat}\beta_{cat}$ versus 8-fold for the full-length enzyme). The K_M for Mn^{2+}-GTP was 85 ± 18 μM (Figure 3C), in good agreement with published values for the full-length enzyme; thus, the difference in activity increase in the presence of Mn^{2+} for $\alpha_{cat}\beta_{cat}$ and the full-length enzyme appears to be due to a change in k_{cat}. The cause of this change remains to be determined.

Dimerization of α_{cat}, β_{cat}, and $\alpha_{cat}\beta_{cat}$. Purified α_{cat} and β_{cat} were subjected to analytical gel filtration on a Pharmacia Superdex 200 column. α_{cat} ran as a mixture of monomer and dimer, with apparent molecular weights of 34 and 70 kDa for the monomer and dimer, respectively, somewhat higher than the calculated molecular weights of 25.9 and 51.8 kDa

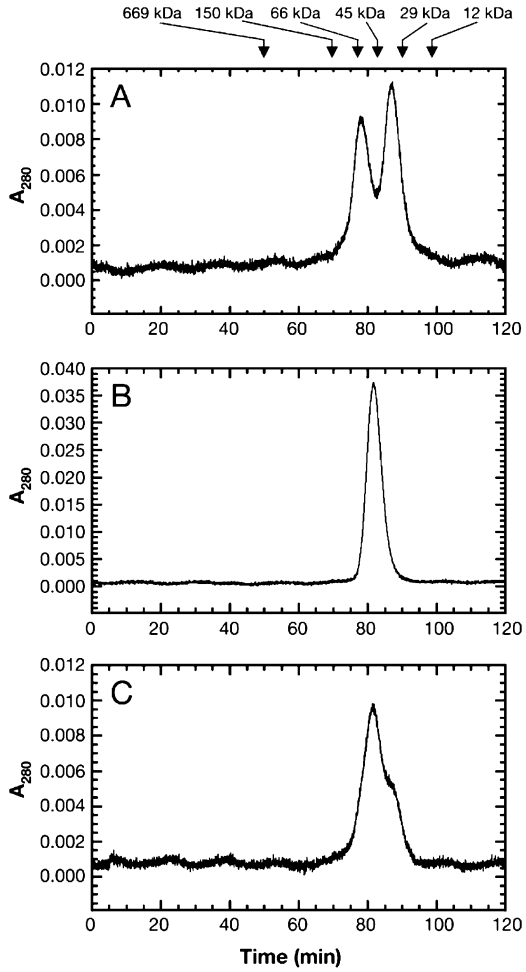

FIGURE 4: Analytical gel filtration profiles of α_{cat}, β_{cat}, and $\alpha_{cat}\beta_{cat}$. α_{cat} (A, 21 μM), β_{cat} (B, 56 μM), and $\alpha_{cat}\beta_{cat}$ (C, 8.9 μM) were gel filtered on a Superdex 200 (HiLoad 16/60) column at 1 mL/min. The positions of elution of molecular weight markers are shown.

(Figure 4A). β_{cat} ran exclusively as a dimer, with an apparent molecular weight of 53 kDa, close to the predicted dimeric weight of 48.2 kDa (Figure 4B). The $\alpha_{cat}\beta_{cat}$ complex ran as mostly dimer, with an apparent molecular weight of 53 kDa, close to the predicted value of 50 kDa (Figure 4C). A small shoulder was observed at ~32 kDa, which likely reflects a slight excess of α_{cat} in the mixture.

Both α_{cat} and β_{cat} were able to homodimerize, thus suggesting that the lack of catalytic activity exhibited by α_{cat} or β_{cat} is due to the inability to form a functional active site without the proper dimeric partner rather than to a lack of dimerization. This is in agreement with the reported properties of the AC catalytic domains (*25*, *34*). The observed mixture of monomer and dimer for α_{cat} suggests that the K_D of the α_{cat} homodimer is in the range of 10−20 μM. Additionally, because 56 μM β_{cat} ran as a dimer, an upper limit for the K_D for the β_{cat} homodimer of 6 μM can be estimated. If the β_{cat} homodimer K_D was 6 μM, then at 60 μM, a monomer/dimer ratio of 1/10 would be expected, and in fact, no monomer was detected in this experiment. Thus, the β_{cat} homodimer has a tighter association (K_D < 6 μM) than does the α_{cat} homodimer ($K_D \approx$ 10−20 μM). The fact that most (if not all) of the $\alpha_{cat}\beta_{cat}$ complex is a dimer at 9 μM indicates that the K_D of the $\alpha_{cat}\beta_{cat}$ heterodimer is close to 0.5−1 μM, lower than that of either the α_{cat} or β_{cat} homodimer. This is consistent with the fact that, for full-length $\alpha 1\beta 1$ enzyme, the primary observed species is the heterodimer.

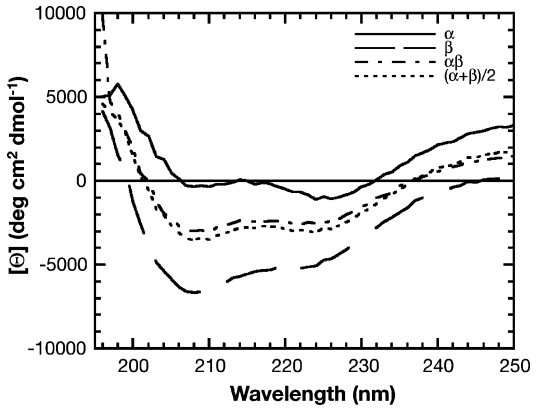

FIGURE 5: Circular dichroism spectra of the sGC catalytic domains. Protein concentrations were α_{cat}, 8.1 μM; β_{cat}, 8.3 μM; and $\alpha_{cat}\beta_{cat}$, 4 μM. While the spectra of α_{cat} and β_{cat} exhibit slight differences from each other, neither protein undergoes a significant change upon formation of the $\alpha_{cat}\beta_{cat}$ complex, as demonstrated by the resemblance of the spectrum of the $\alpha_{cat}\beta_{cat}$ complex to the sum of the spectra of the individual catalytic domains.

Circular dichroism (CD) spectroscopy was used to determine whether a change in secondary structure occurs upon formation of the $\alpha_{cat}\beta_{cat}$ complex (Figure 5). At the concentrations employed in these experiments (8 μM for α_{cat} and β_{cat}, 4 μM for the $\alpha_{cat}\beta_{cat}$ complex), each catalytic domain construct is likely present as a mixture of monomer and dimer, while the $\alpha_{cat}\beta_{cat}$ complex is present as a heterodimer. The CD spectrum of α_{cat} displayed a mixture of α-helical and β-sheet character. The CD spectrum of β_{cat} exhibited a similar mixture with slightly more α-helical character, as seen from the increase in the ratio of A_{209}/A_{222}. The mixture of α-helical and β-sheet characteristics is consistent with secondary structure predictions for the sGC catalytic domains, as well as with the AC crystal structures, which exhibit a $\beta\alpha\beta\beta\alpha\beta$ organization of secondary structure (*35*). The CD spectrum of the $\alpha_{cat}\beta_{cat}$ complex resembles an additive combination of the spectra obtained for α_{cat} and β_{cat}, indicating that no gross changes in secondary structure occur upon heterodimer formation. Taken together with the analytical gel filtration data, the circular dichroism data indicate that the individual catalytic domain constructs fold to stable conformations in the absence of the heterodimeric partner, and these conformations do not change significantly upon heterodimer formation. The inactivity of the α_{cat} or β_{cat} homodimers is most likely due to the lack of key residues, contributed by the heterodimeric partner, that are needed for formation of a catalytically competent active site.

The affinity of the catalytic domain constructs for each other was determined by measuring the specific activity of the complex at different dilutions, with the assumption that activity would decrease as the complex dissociated, allowing the K_D for the complex to be calculated (Figure 6). The activity of varying dilutions of the $\alpha_{cat}\beta_{cat}$ complex was fit to a standard saturation equation, $v = V_{max}[\alpha_{cat}\beta_{cat}]/(K_D + [\alpha_{cat}\beta_{cat}])$, to obtain the K_D of the complex, which was 450 ± 70 nM, in good agreement with the estimate of 0.5−1 μM obtained by gel filtration. The presence of metal and GTP does not appear to affect the formation of heterodimers, as the K_D predicted from the gel filtration studies (0.5−1 μM; in the absence of metal and GTP) matches quite well

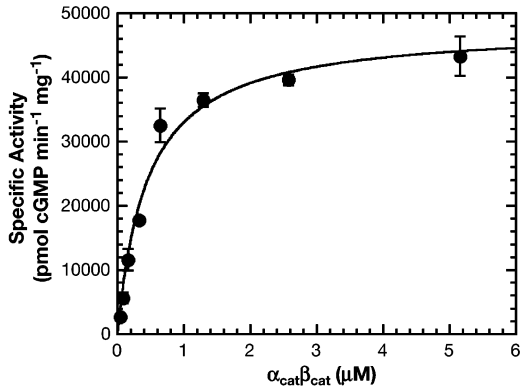

FIGURE 6: Determination of the K_D for the $\alpha_{cat}\beta_{cat}$ complex. Varying amounts of $\alpha_{cat}\beta_{cat}$ complex were assayed for 20 min. Activity of the $\alpha_{cat}\beta_{cat}$ complex was linear with respect to time. The activity data were fit to a standard saturation function, $v = V_{max}$ [$\alpha_{cat}\beta_{cat}$]/(K_D + [$\alpha_{cat}\beta_{cat}$]) to obtain a K_D value of 450 ± 70 nM.

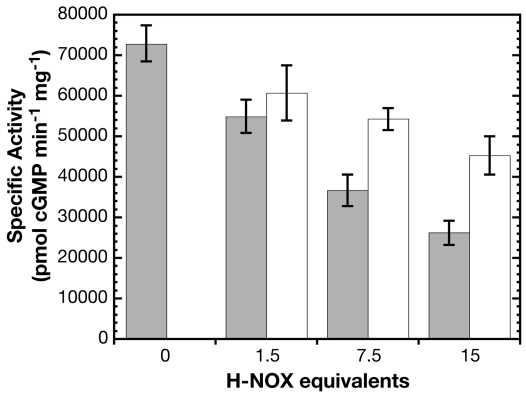

FIGURE 7: Inhibition of the $\alpha_{cat}\beta_{cat}$ complex by heme-binding domain constructs. The activity of 1.6 μM $\alpha_{cat}\beta_{cat}$ complex was inhibited by increasing amounts of the H−NOX domain constructs β1(1−194) (white) and β1(1−385) (dark gray). The amounts of H−NOX domain constructs are shown as molar equivalents relative to the amount of $\alpha_{cat}\beta_{cat}$ complex. β1(1−385), the H−NOX domain construct that also contains the PAS-like domain, inhibited $\alpha_{cat}\beta_{cat}$ activity to a greater extent than did β1(1−194), the construct containing just the H−NOX domain.

with the K_D determined by activity of $\alpha_{cat}\beta_{cat}$ dilutions (450 ± 70 nM; in the presence of metal and GTP). From the gel filtration studies, it can be estimated that the K_D for the β_{cat} homodimer is ~10 times higher than the K_D for the $\alpha_{cat}\beta_{cat}$ heterodimer; thus, under these conditions, the contribution of β_{cat} homodimer formation would be negligible.

Inhibition of $\alpha_{cat}\beta_{cat}$ Activity by sGC Heme-Binding Domain Constructs. The successful expression and purification of active sGC catalytic domain constructs allowed us to examine whether the activity of the $\alpha_{cat}\beta_{cat}$ catalytic domains could be affected by the sGC heme-binding domain in trans. If so, this would be highly suggestive of a direct interaction between the catalytic domains and the heme-binding domain of the enzyme, permitting the possible elucidation of the contacts and mechanisms by which activation of the full-length enzyme by NO occurs. To this end, the $\alpha_{cat}\beta_{cat}$ complex was assayed in the presence of increasing amounts of the sGC heme-binding domain constructs β1(1−194) or β1(1−385). Intriguingly, the activity of the $\alpha_{cat}\beta_{cat}$ catalytic domains was *inhibited* by the heme-binding domain constructs in a concentration-dependent manner (Figure 7). This inhibition was not an artifact of nonspecific protein−protein interactions, as inhibition did not occur with equivalent amounts of bovine serum albumin or immunoglobulin G, nor was it an effect due to the presence of Mn^{2+} in the assays, as similar inhibition was observed in the presence of Mg^{2+} (data not shown). As seen in Figure 7, the inhibition of the activity of the $\alpha_{cat}\beta_{cat}$ complex by the homodimeric heme-binding domain construct β1(1−385) (*22*) was greater than that observed for the monomeric construct β1(1−194). The inhibition by either heme-binding domain construct was unaffected by the presence of 100 μM DEA/NO (data not shown).

These observations indicate that the N-terminal heme-binding domain of sGC can interact with one or both of the catalytic domains in the full-length enzyme and suggest that the function of the N-terminus of the β1 subunit of sGC may be to act as an autoinhibitory domain, whose inhibition is relieved upon binding of NO to the heme-binding domain, resulting in an increase in enzyme activity. We were unable to examine the effect of the α1 N-terminal domain on the activity of the $\alpha_{cat}\beta_{cat}$ heterodimer because of difficulties expressing the α1 N-terminal domain in a soluble form. It is possible that the α1 N-terminal domain may exert an effect on the activity of the catalytic domains; however, this is unlikely because the region of the α1 N-terminus corresponding to the β1 heme-binding domain can be deleted without much effect on the activity or NO-activation of sGC (*11*).

Significantly, the primary difference between β1(1−194) and β1(1−385) is that the longer construct, which appears to be a more potent inhibitor, contains the central domain of the β1 subunit, which is predicted to adopt a PAS-like fold (*7*). When it occurs in other proteins, the PAS domain often mediates protein−protein interactions. These interactions are modulated by a large number of factors, including light, gases, redox chemistry, and the binding of small molecules (*7*, *36*−*38*). Interestingly, the PAS-like regions of the α1 and β1 subunit of sGC are more conserved between the subunits than are the N-terminal regions (45% identity and 65% similarity for the PAS-like domains versus 20% identity and 47% similarity for the N-terminal domains) (*39*), suggesting that these domains are crucial to the proper functioning of the enzyme. Finally, recent structural and mutational studies describe a relevant mammalian signaling system: the function of the PAS domain of the human PAS kinase is autoinhibitory, and addition of the isolated PAS domain to the truncated kinase domain results in specific and concentration-dependent inhibition of kinase activity in trans (*37*, *38*). Thus, taken together, the data and observations described above suggest a domain-scale mechanism for how activation of sGC is achieved (Figure 8): NO binds to the heme of the N-terminal heme-binding domain, causing a conformational change that, mediated and perhaps amplified by the PAS domains, is transmitted to the catalytic domains. This conformational change causes relief of an inhibitory interaction and allows the catalytic domains to shift relative to one another, bringing active site residues into an optimum alignment for maximum activity. Currently, the molecular mechanism by which the N-terminal domains of sGC interact with the catalytic domains is unknown. It is tempting to propose that the heme-binding domain of sGC interacts at the interface of α_{cat} and β_{cat} to exert its effect on enzyme activity, in a manner similar to that proposed for the regulation of the catalytic domains of mammalian AC by

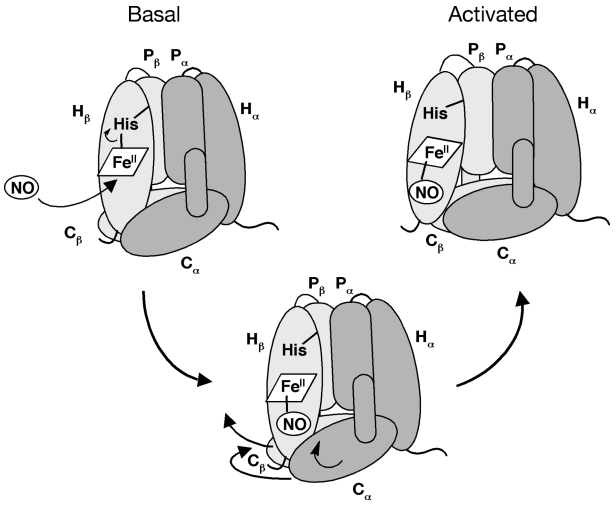

FIGURE 8: A domain-scale mechanism for the activation of sGC by NO. NO binds to the sGC heme, breaking the iron−histidine bond to form the five-coordinate ferrous−nitrosyl complex. The change in the heme environment causes a conformational change in the H−NOX domain. This change results in the movement of the heme domain away from the catalytic domains. The catalytic domains are then free to shift relative to one another, which brings crucial catalytic residues into the proper alignment for enzyme activity.

$G_{s\alpha}$ (*34*, *35*); however, further experimentation will be necessary to distinguish between this mechanism and others.

ACKNOWLEDGMENT

We thank Natalie Pao for assistance with protein expression, Eric Schneider for assistance with CD spectroscopy, the Marqusee lab for the use of their CD spectrophotometer, Stephen Cary for insightful discussion, and the Marletta lab for critical reading of this manuscript.

REFERENCES

1. Ignarro, L. J. (1989) Heme-dependent activation of soluble guanylate cyclase by nitric oxide: regulation of enzyme activity by porphyrins and metalloporphyrins, *Semin. Hematol. 26*, 63−76.
2. Yuen, P. S., and Garbers, D. L. (1992) Guanylyl cyclase-linked receptors, *Annu. Rev. Neurosci. 15*, 193−225.
3. Denninger, J. W., and Marletta, M. A. (1999) Guanylate cyclase and the •NO/cGMP signaling pathway, *Biochim. Biophys. Acta 1411*, 334−350.
4. Wedel, B., and Garbers, D. (2001) The guanylyl cyclase family at Y2K, *Annu. Rev. Physiol. 63*, 215−233.
5. Friebe, A., and Koesling, D. (2003) Regulation of nitric oxide-sensitive guanylyl cyclase, *Circ. Res. 93*, 96−105.
6. Munzel, T., Feil, R., Mulsch, A., Lohmann, S. M., Hofmann, F., and Walter, U. (2003) Physiology and pathophysiology of vascular signaling controlled by guanosine 3′,5′-cyclic monophosphate-dependent protein kinase, *Circulation 108*, 2172−2183.
7. Iyer, L. M., Anantharaman, V., and Aravind, L. (2003) Ancient conserved domains shared by animal soluble guanylyl cyclases and bacterial signaling proteins, *BMC Genomics 4*, 5.
8. Pellicena, P., Karow, D. S., Boon, E. M., Marletta, M. A., and Kuriyan, J. (2004) Crystal structure of an oxygen binding heme domain related to soluble guanylate cyclases, *Proc. Natl. Acad. Sci. U.S.A. 101*, 12854−12859.
9. Stone, J. R., and Marletta, M. A. (1995) Heme stoichiometry of heterodimeric soluble guanylate cyclase, *Biochemistry 34*, 14668−14674.
10. Stone, J. R., and Marletta, M. A. (1996) Spectral and kinetic studies on the activation of soluble guanylate cyclase by nitric oxide, *Biochemistry 35*, 1093−1099.
11. Koglin, M., and Behrends, S. (2003) A functional domain of the alpha1 subunit of soluble guanylyl cyclase is necessary for activation of the enzyme by nitric oxide and YC-1 but is not involved in heme binding, *J. Biol. Chem. 278*, 12590−12597.
12. Zhou, Z., Gross, S., Roussos, C., Meurer, S., Muller-Esterl, W., and Papapetropoulos, A. (2004) Structural and functional characterization of the dimerization region of soluble guanylyl cyclase, *J. Biol. Chem. 279*, 24935−24943.
13. Wedel, B., Harteneck, C., Foerster, J., Friebe, A., Schultz, G., and Koesling, D. (1995) Functional domains of soluble guanylyl cyclase, *J. Biol. Chem. 270*, 24871−24875.
14. Tang, W. J., and Gilman, A. G. (1992) Adenylyl cyclases, *Cell 70*, 869−872.
15. Garbers, D. L., and Lowe, D. G. (1994) Guanylyl cyclase receptors, *J. Biol. Chem. 269*, 30741−30744.
16. Hoenicka, M., Becker, E. M., Apeler, H., Sirichoke, T., Schroder, H., Gerzer, R., and Stasch, J. P. (1999) Purified soluble guanylyl cyclase expressed in a baculovirus/Sf9 system: stimulation by YC-1, nitric oxide, and carbon monoxide, *J. Mol. Med. 77*, 14−23.
17. Garbers, D. L. (1979) Purification of soluble guanylate cyclase from rat lung, *J. Biol. Chem. 254*, 240−243.
18. Stone, J. R., and Marletta, M. A. (1994) Soluble guanylate cyclase from bovine lung: activation with nitric oxide and carbon monoxide and spectral characterization of the ferrous and ferric states, *Biochemistry 33*, 5636−5640.
19. Wolin, M. S., Wood, K. S., and Ignarro, L. J. (1982) Guanylate cyclase from bovine lung, *J. Biol. Chem. 257*, 13312−13320.
20. Mulsch, A., and Gerzer, R. (1991) Purification of heme-containing soluble guanylyl cyclase, *Methods Enzymol. 195*, 377−383.
21. Buechler, W., Singh, S., Aktas, J., Muller, S., Murad, F., and Gerzer, R. (1995) High-level expression of biologically active soluble guanylate cyclase using the baculovirus system is strongly heme-dependent, *Adv. Pharmacol. 34*, 293−303.
22. Zhao, Y., and Marletta, M. A. (1997) Localization of the heme binding region of soluble guanylate cyclase, *Biochemistry 36*, 15959−15964.
23. Tang, W. J., and Gilman, A. G. (1995) Construction of a soluble adenylyl cyclase activated by Gs alpha and forskolin, *Science 268*, 1769−1772.
24. Yan, S. Z., Hahn, D., Huang, Z. H., and Tang, W. J. (1996) Two cytoplasmic domains of mammalian adenylyl cyclase form a Gs alpha- and forskolin-activated enzyme in vitro, *J. Biol. Chem. 271*, 10941−10945.
25. Whisnant, R. E., Gilman, A. G., and Dessauer, C. W. (1996) Interaction of the two cytosolic domains of mammalian adenylyl cyclase, *Proc. Natl. Acad. Sci. U.S.A. 93*, 6621−6625.
26. Artz, J. D., Schmidt, B., McCracken, J. L., and Marletta, M. A. (2002) Effects of nitroglycerin on soluble guanylate cyclase: implications for nitrate tolerance, *J. Biol. Chem. 277*, 18253−18256.
27. Zhao, Y., Brandish, P. E., DiValentin, M., Schelvis, J. P., Babcock, G. T., and Marletta, M. A. (2000) Inhibition of soluble guanylate cyclase by ODQ, *Biochemistry 39*, 10848−10854.
28. Hatley, M. E., Gilman, A. G., and Sunahara, R. K. (2002) Expression, purification, and assay of cytosolic (catalytic) domains of membrane-bound mammalian adenylyl cyclases, *Methods Enzymol. 345*, 127−140.
29. Xu, Z., Horwich, A. L., and Sigler, P. B. (1997) The crystal structure of the asymmetric GroEL-GroES-(ADP)7 chaperonin complex, *Nature 388*, 741−750.
30. Harteneck, C., Koesling, D., Soling, A., Schultz, G., and Bohme, E. (1990) Expression of soluble guanylyl cyclase: Catalytic activity requires two enzyme subunits, *FEBS Lett. 272*, 221−223.
31. Buechler, W. A., Nakane, M., and Murad, F. (1991) Expression of soluble guanylate cyclase activity requires both enzyme subunits, *Biochem. Biophys. Res. Commun. 174*, 351−357.
32. Lee, Y. C., Martin, E., and Murad, F. (2000) Human recombinant soluble guanylyl cyclase: expression, purification, and regulation, *Proc. Natl. Acad. Sci. U.S.A. 97*, 10763−10768.
33. Waldman, S. A., and Murad, F. (1987) Cyclic GMP synthesis and function, *Pharmacol. Rev. 39*, 163−196.
34. Sunahara, R. K., Dessauer, C. W., Whisnant, R. E., Kleuss, C., and Gilman, A. G. (1997) Interaction of Gsalpha with the cytosolic domains of mammalian adenylyl cyclase, *J. Biol. Chem. 272*, 22265−22271.
35. Tesmer, J. J., Sunahara, R. K., Gilman, A. G., and Sprang, S. R. (1997) Crystal structure of the catalytic domains of adenylyl

cyclase in a complex with Gsalpha.GTPgammaS, *Science 278*, 1907−1916.
36. Hefti, M. H., Francoijs, K. J., de Vries, S. C., Dixon, R., and Vervoort, J. (2004) The PAS fold: a redefinition of the PAS domain based upon structural prediction, *Eur. J. Biochem. 271*, 1198−1208.
37. Rutter, J., Michnoff, C. H., Harper, S. M., Gardner, K. H., and McKnight, S. L. (2001) PAS kinase: an evolutionarily conserved PAS domain-regulated serine/threonine kinase, *Proc. Natl. Acad. Sci. U.S.A. 98*, 8991−8996.
38. Amezcua, C. A., Harper, S. M., Rutter, J., and Gardner, K. H. (2002) Structure and interactions of PAS kinase N-terminal PAS domain: model for intramolecular kinase regulation, *Structure 10*, 1349−1361.
39. Stone, J. R. (1997) Ph.D. Thesis, The University of Michigan, Ann Arbor, MI.
40. Taussig, R., and Gilman, A. G. (1995) Mammalian membrane-bound adenylyl cyclases, *J. Biol. Chem. 270*, 1−4.

BI047601D